UNCLASSIFIED

AD

Technical Report DEVCOMAC-BLTR-22004

Laser-induced Surface Structuring for Enhanced Surface Performance

Strategic Environmental Research and Development Program (SERDP) Project WP-2753
Final Report

Dr. Jeffrey M. Warrender

U.S. Army Combat Capabilities
Development Command Armaments Center
Weapons and Software Engineering Center
Benét Laboratories
Watervliet, NY 12189

2022-January-31

UNCLASSIFIED//DISTRIBUTION STATEMENT A. Approved for public release; distribution is unlimited.

The views, opinions, and/or findings contained in this report are those of the author(s) and should not be construed as an official Department of the Army position, policy, or decision, unless so designated by other documentation.

The citation in this report of the names of commercial firms or commercially available products or services does not constitute official endorsement by or approval of the U.S. Government.

Destroy this report when no longer needed by any method that will prevent disclosure of its contents or reconstruction of the document. Do not return to the originator.

REPORT DOCUMENTATION PAGE

Form Approved
OMB No. 0704-0188

1. REPORT DATE *(DD-MM-YYYY)*
12/21/2021

2. REPORT TYPE
Final Report

3. DATES COVERED *(From - To)*

4. TITLE AND SUBTITLE
Laser-induced Surface Structuring for Enhanced Surface Performance

5a. CONTRACT NUMBER

5b. GRANT NUMBER

5c. PROGRAM ELEMENT NUMBER

6. AUTHOR(S)
Jeffrey M. Warrender

5d. PROJECT NUMBER

5e. TASK NUMBER

5f. WORK UNIT NUMBER

7. PERFORMING ORGANIZATION NAME(S) AND ADDRESS(ES)
U.S. Army Combat Capabilities Development Command Armaments Center
Weapons and Software Engineering Center, Benét Laboratories
1 Buffington Street
Watervliet, NY 12189

8. PERFORMING ORGANIZATION REPORT NUMBER
DEVCOMAC-BLTR-22004

9. SPONSORING/MONITORING AGENCY NAME(S) AND ADDRESS(ES)
U.S. Army Combat Capabilities Development Command Armaments Center
Weapons and Software Engineering Center, Benét Laboratories
1 Buffington Street
Watervliet, NY 12189

10. SPONSOR/MONITOR'S ACRONYM(S)

11. SPONSOR/MONITOR'S REPORT NUMBER(S)

12. DISTRIBUTION/AVAILABILITY STATEMENT
Distribution Statement A. Approved for public release; distribution is unlimited.

13. SUPPLEMENTARY NOTES
Strategic Environmental Research and Development Program (SERDP) Project WP-2753
Journal of Applied Physics

14. ABSTRACT
Steel and aluminum test panels were irradiated with large numbers of pulses from a Nd:YAG (532 nm) or KrF excimer (248 nm) at fluence between 0.3 and 3.0 J/cm2, which induced changes to the surface topography of the panels. In most cases this led to considerable roughening of the surface, and decoration of the roughened surface with nanoscale particles. The contact angle of water droplets was measured, and showed both increased and decreased contact angle compared to unshot material, depending on the laser conditions. The changes to the surface hydrophobicity are non-monotonic in both laser fluence and shot density. Comparisons against surface topography suggest that the surfaces that exhibit two length s

15. SUBJECT TERMS
Laser, surface structuring

16. SECURITY CLASSIFICATION OF: a. REPORT	b. ABSTRACT	c. THIS PAGE	17. LIMITATION OF ABSTRACT	18. NUMBER OF PAGES	19a. NAME OF RESPONSIBLE PERSON
					Jeffrey M. Warrender
					19b. TELEPHONE NUMBER *(Include area code)*
U	SAR	SAR	SAR	25	518-937-7157

INSTRUCTIONS FOR COMPLETING SF 298

1. REPORT DATE. Full publication date, including day, month, if available. Must cite at least the year and be Year 2000 compliant, e.g. 30-06-1998; xx-06-1998; xx-xx-1998.

2. REPORT TYPE. State the type of report, such as final, technical, interim, memorandum, master's thesis, progress, quarterly, research, special, group study, etc.

3. DATE COVERED. Indicate the time during which the work was performed and the report was written, e.g., Jun 1997 - Jun 1998; 1-10 Jun 1996; May - Nov 1998; Nov 1998.

4. TITLE. Enter title and subtitle with volume number and part number, if applicable. On classified documents, enter the title classification in parentheses.

5a. CONTRACT NUMBER. Enter all contract numbers as they appear in the report, e.g. F33315-86-C-5169.

5b. GRANT NUMBER. Enter all grant numbers as they appear in the report. e.g. AFOSR-82-1234.

5c. PROGRAM ELEMENT NUMBER. Enter all program element numbers as they appear in the report, e.g. 61101A.

5e. TASK NUMBER. Enter all task numbers as they appear in the report, e.g. 05; RF0330201; T4112.

5f. WORK UNIT NUMBER. Enter all work unit numbers as they appear in the report, e.g. 001; AFAPL30480105.

6. AUTHOR(S). Enter name(s) of person(s) responsible for writing the report, performing the research, or credited with the content of the report. The form of entry is the last name, first name, middle initial, and additional qualifiers separated by commas, e.g. Smith, Richard, J, Jr.

7. PERFORMING ORGANIZATION NAME(S) AND ADDRESS(ES). Self-explanatory.

8. PERFORMING ORGANIZATION REPORT NUMBER. Enter all unique alphanumeric report numbers assigned by the performing organization, e.g. BRL-1234; AFWL-TR-85-4017-Vol-21-PT-2.

9. SPONSORING/MONITORING AGENCY NAME(S) AND ADDRESS(ES). Enter the name and address of the organization(s) financially responsible for and monitoring the work.

10. SPONSOR/MONITOR'S ACRONYM(S). Enter, if available, e.g. BRL, ARDEC, NADC.

11. SPONSOR/MONITOR'S REPORT NUMBER(S). Enter report number as assigned by the sponsoring/ monitoring agency, if available, e.g. BRL-TR-829; -215.

12. DISTRIBUTION/AVAILABILITY STATEMENT. Use agency-mandated availability statements to indicate the public availability or distribution limitations of the report. If additional limitations/ restrictions or special markings are indicated, follow agency authorization procedures, e.g. RD/FRD, PROPIN, ITAR, etc. Include copyright information.

13. SUPPLEMENTARY NOTES. Enter information not included elsewhere such as: prepared in cooperation with; translation of; report supersedes; old edition number, etc.

14. ABSTRACT. A brief (approximately 200 words) factual summary of the most significant information.

15. SUBJECT TERMS. Key words or phrases identifying major concepts in the report.

16. SECURITY CLASSIFICATION. Enter security classification in accordance with security classification regulations, e.g. U, C, S, etc. If this form contains classified information, stamp classification level on the top and bottom of this page.

17. LIMITATION OF ABSTRACT. This block must be completed to assign a distribution limitation to the abstract. Enter UU (Unclassified Unlimited) or SAR (Same as Report). An entry in this block is necessary if the abstract is to be limited.

ABSTRACT

Steel and aluminum test panels were irradiated with large numbers of pulses from a Nd:YAG (532 nm) or KrF excimer (248 nm) at fluence between 0.3 and 3.0 J/cm2, which induced changes to the surface topography of the panels. In most cases this led to considerable roughening of the surface, and decoration of the roughened surface with nanoscale particles. The contact angle of water droplets was measured, and showed both increased and decreased contact angle compared to unshot material, depending on the laser conditions. The changes to the surface hydrophobicity are non-monotonic in both laser fluence and shot density. Comparisons against surface topography suggest that the surfaces that exhibit two length scales of roughness are more likely to be excessively hydrophobic, whereas surfaces that have large scale features are more likely to be excessively hydrophilic.

Table of Contents

List of Figures

Introduction

The pervasive use of metallic components in military applications is understandable, because of the beneficial structural properties that metals provide. Metallic *surfaces*, however, present numerous challenges, and the greatest of these is often their interaction with the component's service environment. In some cases, the extreme conditions characteristic of military use present materials challenges (*e.g*. the bore surface of a gun tube can degrade due to the high temperatures achieved during firing). However, in many cases, it is exposure to the ambient environment that threatens the material, and this commonly occurs in the form of *environmental corrosion* and *biological contamination*. Systems with large surface areas, such as aircraft airframes, vehicle bodies, and ship hulls, are particularly susceptible to such concerns.

The most common metals in military use, steel and aluminum (and its alloys) are susceptible to environmental corrosion. To protect the metal substrate, coatings are frequently applied to the substrate. Unfortunately, most coatings either require the use of toxic chemicals (such as hard chrome), are themselves toxic (such as cadmium), or require toxic chemical pre-treatments, such as those described in MIL-PRF-32239. These coatings expose personnel to hazardous chemicals, in the coating application, repair processes, the service environment, or all of these situations.[1] Additionally, these processes generate considerable toxic waste. As a result, elimination of pre-treatments that make use of toxic chemicals would be advantageous. To accomplish new benign methods for the preparation of surfaces for the application of adhesive coatings is critical.

The problem of biological contamination is fundamentally different; instead of promoting adhesion to the surface, one wishes to prevent it. Particularly challenging examples include mold growth on weapon systems and biofouling of Navy ship hulls. Such biofouling can take the form of the formation of a film or attachment of soft coatings, or, more problematic, the attachment of hard species such as mollusks and barnacles.[2-4] The attachment of such species result in severely degraded performance (estimates place the additional fuel consumption resulting from barnacle-caused drag as high as 40%) and removal upon attachment is difficult. To combat this, in the past, the Navy has treated ship hulls with coatings toxic to barnacles; however, these coatings are also toxic to all species in the aquatic environment and, thus, have an enormous environmental impact.[2]

Our project sought to replace the use of harsh chemical treatments with physical modification to the surface. The introduction of surface topography can have beneficial effects in the case of paint coating adhesion, by allowing entanglement of nano- and microtopographic features with polymerizable and crosslinkable components of the paint. On the other hand, surface topographical features are known in nature to suppress adhesion, the classic example being the self-cleaning Lotus leaf. A key characteristic is the interaction of the *length scale* of the topographic features in comparison to the length scale of the features of the coating in question.[5]

In particular, laser irradiation has been shown to induce microstructural and chemical changes in surfaces, which can enhance their optical absorption [6], tribological performance [7], corrosion-resistance [8-10], or hydrophobicity [12-13]. The effect that a laser will have on a given target is complicated, and depends on the laser's pulse duration and intensity, as well as on the initial microstructure and properties of the target. At low intensity, the laser may melt the surface, which can be used to induce surface alloying [11] or to remove deleterious second-phase particles in alloyed metals [9]. At higher instantaneous intensities, achieved with short pulse duration lasers, athermal processes begin to be important, and ejection of material via formation of a hot, dense plasma is observed. If performed in liquid, this creates shock waves that "peen" the surface, which can improve its corrosion resistance[10]; in air or in vacuum, ablation of material can lead to surface microstructures qualitatively described as "spikes" or "bumps", which improve hydrophobicity by reducing the ability of a water drop to spread out as it would on a flat metal surface.[9] Hydrophobic surfaces have attracted great attention in recent years as potential "self-cleaning" surfaces, with improved resistance to biological contamination, and the similar behavior of the small-scale (~10 micron) "protrusions" on the leaves of the Lotus plant inspire and motivate the search for similar behavior in metal substrates.[13] For corrosion problems in which extended contact with hygroscopic substances is likely, improved hydrophobicity may improve a coating's corrosion resistance as well.

Preliminary data in our lab had previously shown a factor-of-3 reduction in corrosion mass loss for steel samples treated with a laser-structuring process compared to untreated steel. We have also found, consistent with the literature, that the laser irradiations of steel induce features on several length scales: there are "macro" scale features determined by the size of the laser spot, but these are decorated with smaller sub-micron scale protrusions which are themselves decorated with tens-of-nanometer-scale roughness. The topography changes depending on the laser parameters – the intensity, the number of shots hitting an area, and the spacing between shots.

Experimental

We obtained test panels of 3003-H14 aluminum and 4340 steel (Q-Labs Corp). The panels were placed horizontally on a motorized stage and rastered under the focused beam of either a KrF laser (248 nm, 15 ns pulse) or a frequency-double Nd:YAG laser (532 nm, 6 ns pulse). The former produces a rectangular spot approximately 2 mm by 1 mm; the latter produces a circular spot 1.3 mm in diameter. The translation speed of the stage was varied, relative to the pulsing frequency of the laser, so as to controllably vary the average number of laser shots that would hit a given area of the sample. For each specimen, an area at least 1 cm^2 was irradiated. The laser fluence was also systematically varied, by adjusting the output energy of the laser.

Nd:YAG irradiations were performed at 0.27, 1.15, and 2.3 J/cm^2. The shot densities were 80, 120, 310, and 820 shots per area. Excimer laser irradiations were performed at

0.3, 1.0, 1.5, and 3.0 J/cm^2. The shot densities were 375, 750, 1000, 1500, and 3000 shots per area.

The topography of the samples post-irradiation was examined with an electron microscope (FEI Helios Nanolab) at 20 kV, with measurements made in the secondary electron detector, at magnification from 350× to 35,000×.

The contact angle of a water droplet placed on the surface was measured with a contact angle meter (Attension), to determine the hydrophobicity of the material pre- and post-irradiation. Unirradiated areas of each sample were measured as a control. Measurements were made with deionized water. The water was dropped onto the irradiated area and monitored with a camera for several seconds, then the surface was blown clean prior to the next droplet. The software fits the droplet image to a spherical cap to determine the contact angle. Each irradiated area was measured between 3 and 5 times, and the measurements were averaged to determine the contract angle.

Results

Fig. 1 and Fig. 2 show contour plots for the contact angle after irradiation by excimer (Fig. 1) and Nd:YAG (Fig. 2), respectively. The contact angle for unshot material appears in the color bar for reference. As can be seen, both sets of excimer-irradiated samples show areas where the contact angle has increased, indicating that the surface has become more hydrophobic, and other regions where the contact angle has decreased, indicating that the surface has become more hydrophilic.

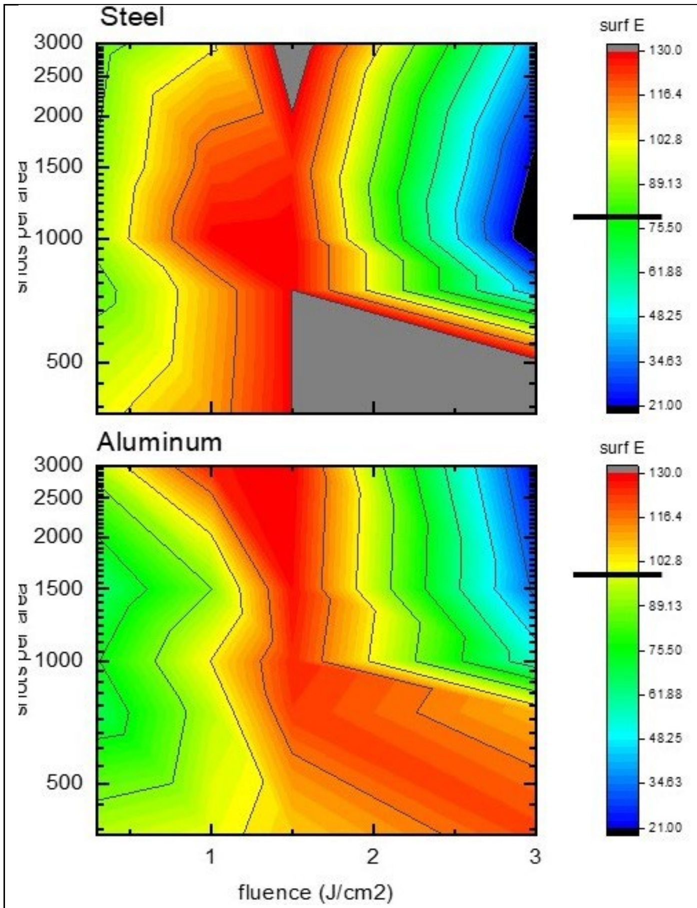

Fig.1 Contact angle contour plot for steel (top) and aluminum (bottom) panels irradiated with a KrF excimer laser at varying laser fluence and shots per area. The black line shows the baseline contact angle for unirradiated material.

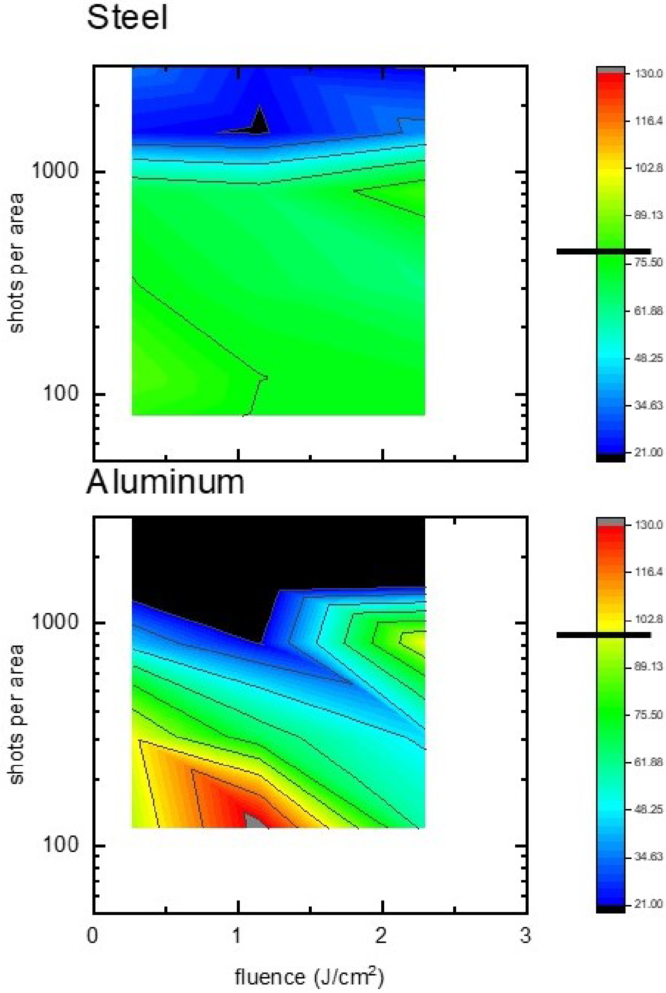

Fig.2 Contact angle contour plot for steel (top) and aluminum (bottom) panels irradiated with an Nd:YAG laser at varying laser fluence and shots per area. The black line shows the baseline contact angle for unirradiated material.

SEM images show the surface topography that resulted in the various surface conditions. First we consider excimer-shot Al samples. Fig. 3 shows a fluence series at constant shot density, akin to taking a horizontal slice across Fig. 1. The images in Fig. 3 were taken at low resolution, and show the large scale features the samples exhibit. At higher resolution, as was the case for Fig. 4 and Fig. 5, fine features decorating the coarser-scale undulations are visible, becoming larger and more pronounced at higher fluence. Holding the fluence constant and increasing the shot density shows a similar progression, as in Fig. 6; the overall roughness of the surface increases as does the size of the representative surface features.

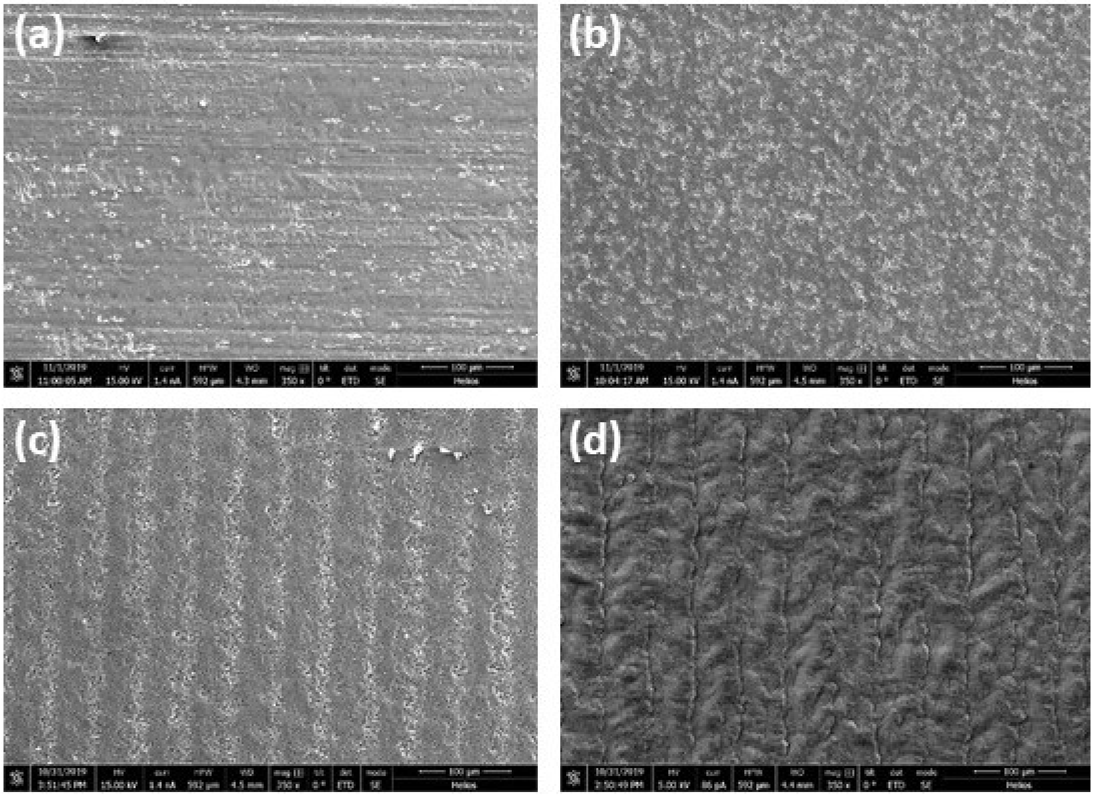

Fig. 3. Excimer-shot Al irradiated with 1500 shots per area at (a) 0.3 J/cm^2, (b) 1.0 J/cm^2, (c) 1.5 J/cm^2 and (d) 3.0 J/cm^2, all at 350× magnification.

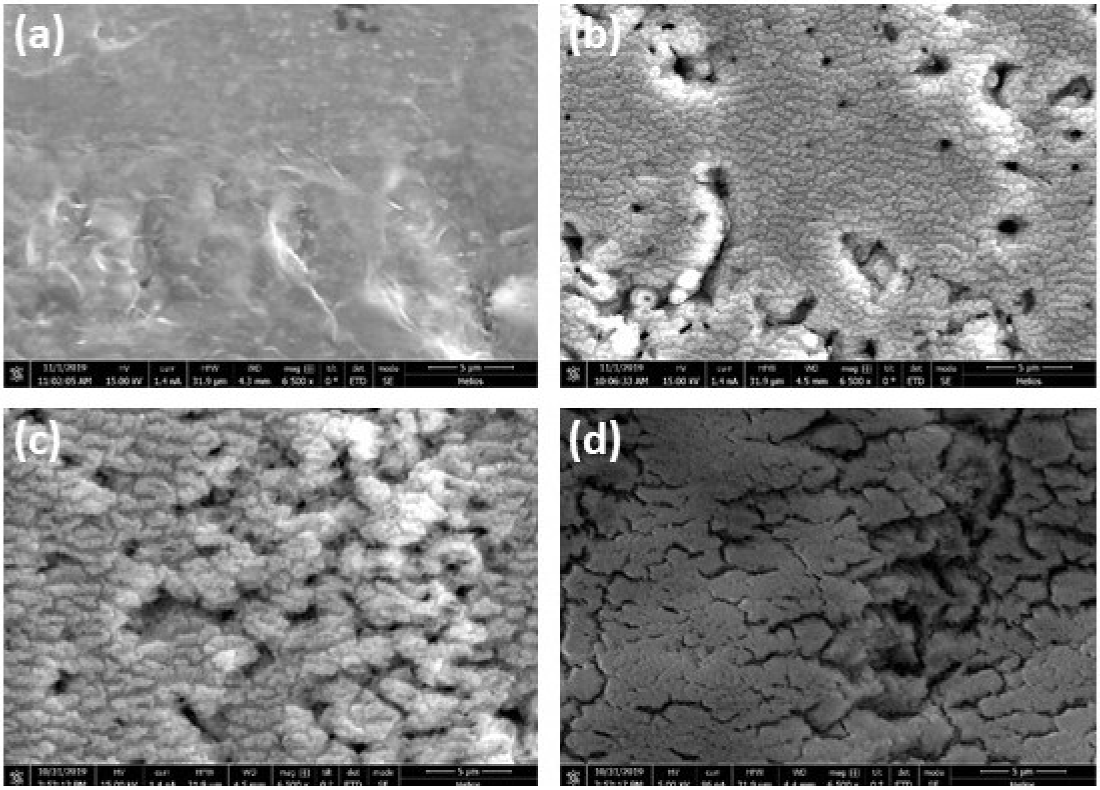

Fig. 4. Excimer-shot Al irradiated with 1500 shots per area at (a) 0.3 J/cm^2, (b) 1.0 J/cm^2, (c) 1.5 J/cm^2 and (d) 3.0 J/cm^2, all at 6500× magnification.

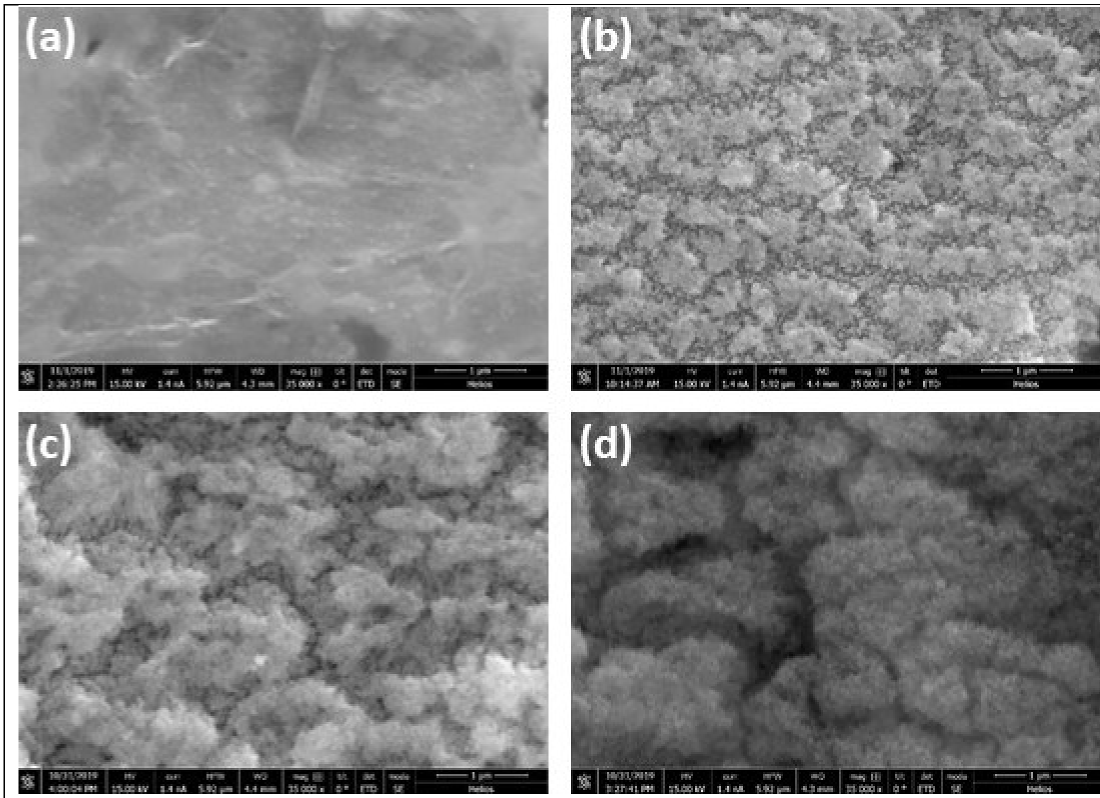

Fig. 5. Excimer-shot Al irradiated with 1000 shots per area at (a) 0.3 J/cm^2, (b) 1.0 J/cm^2, (c) 1.5 J/cm^2 and (d) 3.0 J/cm^2, all at 35,000× magnification.

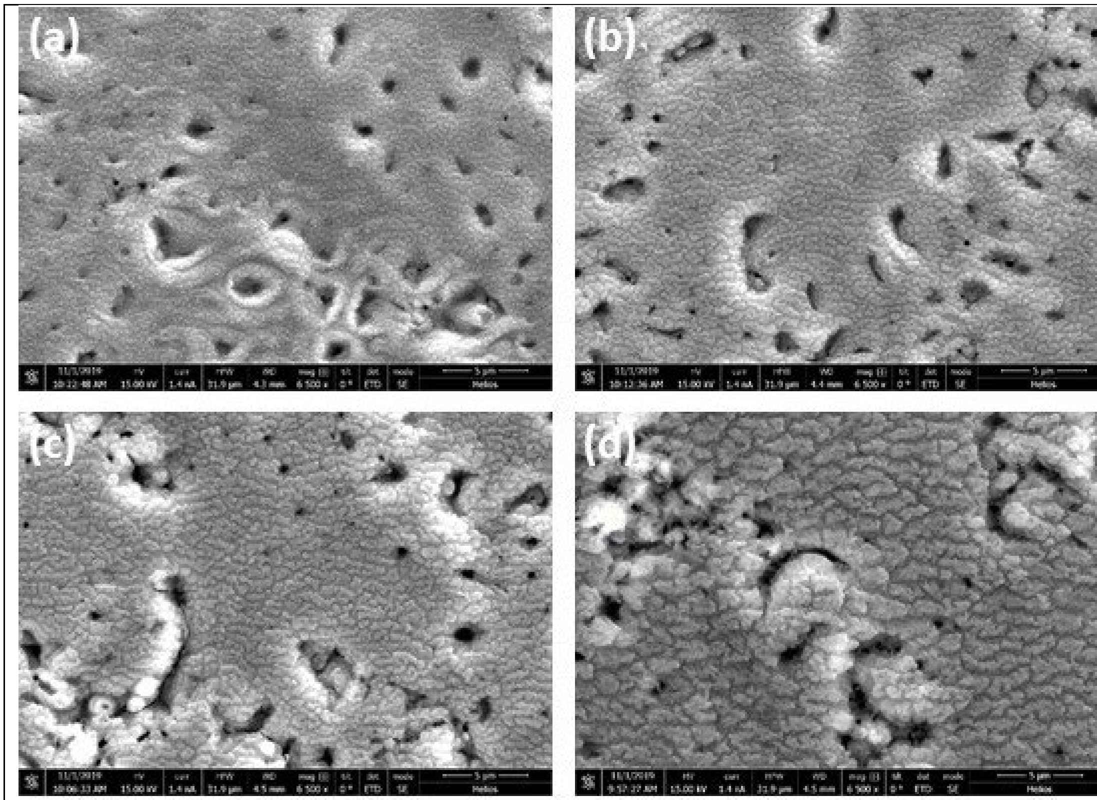

Fig. 6. Excimer-shot Al irradiated at 1 J/cm^2, with (a) 750, (b) 1000, (c) 1500, and (d) 3000 shots per area, all at 6500× magnification.

Excimer-shot steel samples show some similarities. Fig. 7 and Fig. 8 show representative images from varying the laser fluence and shot density, respectively. In Fig. 7, the qualitative appearance of the surface topography is dramatically different between the lowest and highest fluence, whereas in Fig. 8, the images are qualitatively similar, with larger undulations decorated by small features, but the length scale increases considerably as the shot density increases.

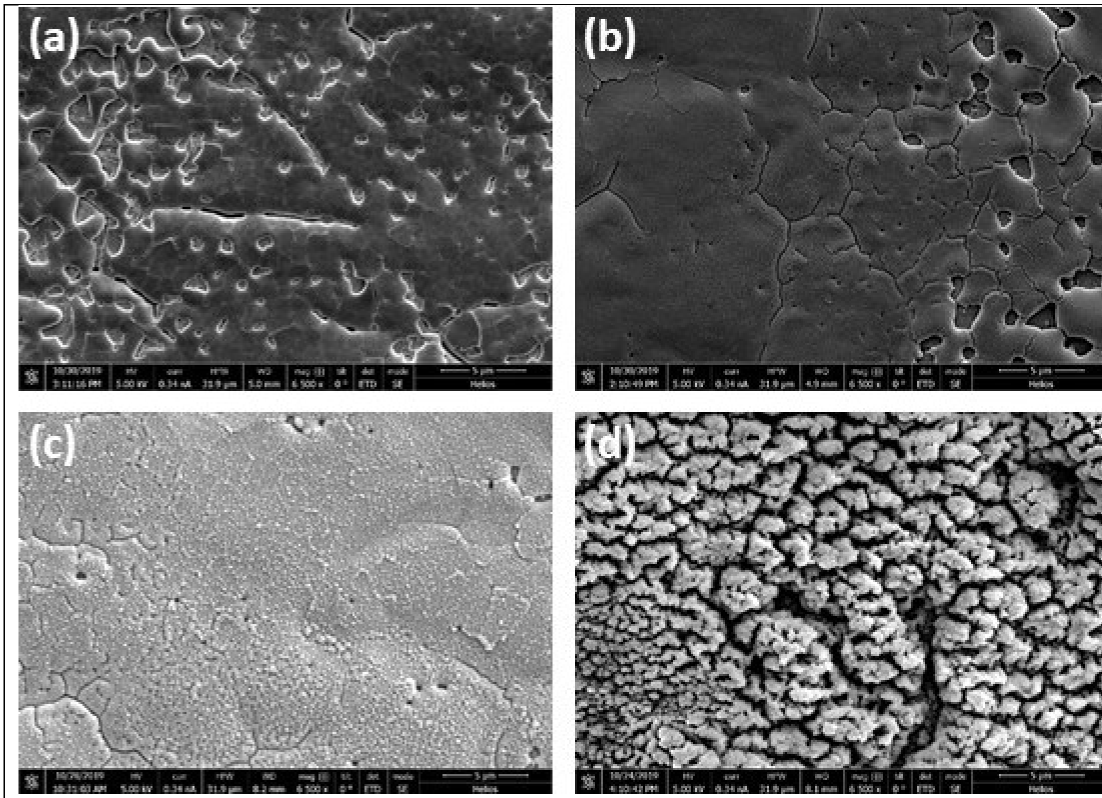

Fig. 7. Excimer-shot steel irradiated with 750 shots per area at (a) 0.3 J/cm^2, (b) 1.0 J/cm^2, (c) 1.5 J/cm^2 and (d) 3.0 J/cm^2, all at 6500× magnification.

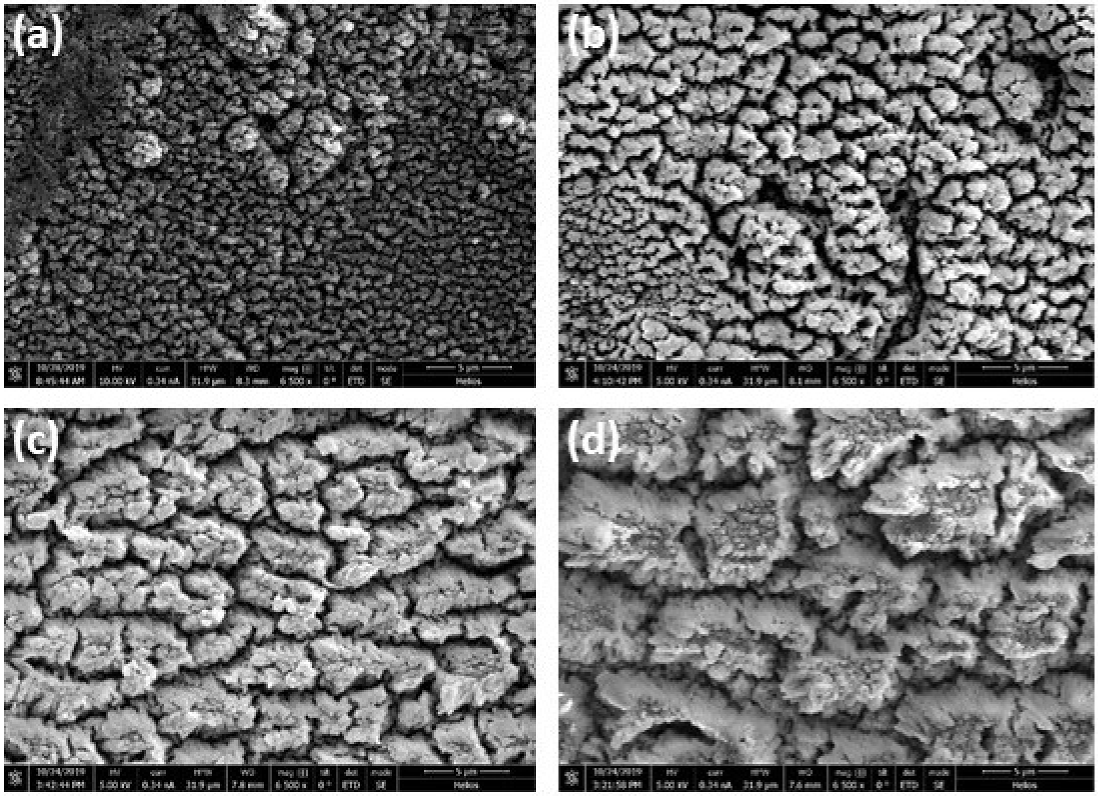

Fig. 8. Excimer-shot steel irradiated at 3 J/cm^2 with (a) 375, (b) 750, (c) 1500 and (d) 3000 shots per area, all at 6500× magnification.

Fig. 9 and Fig. 10 show similar evolutions for Nd:YAG irradiations of steel, varying the laser fluence and shot density, respectively. Although some similar trends are evident, the overall topographic appearance of these samples is quite different from irradiations at 248 nm. In Fig. 11 and 12, a similar progression for Al samples that, like the steel, little resembles the progressions for KrF, even taking into account that the shot densities are lower for the Nd:YAG samples than for most of the KrF samples.

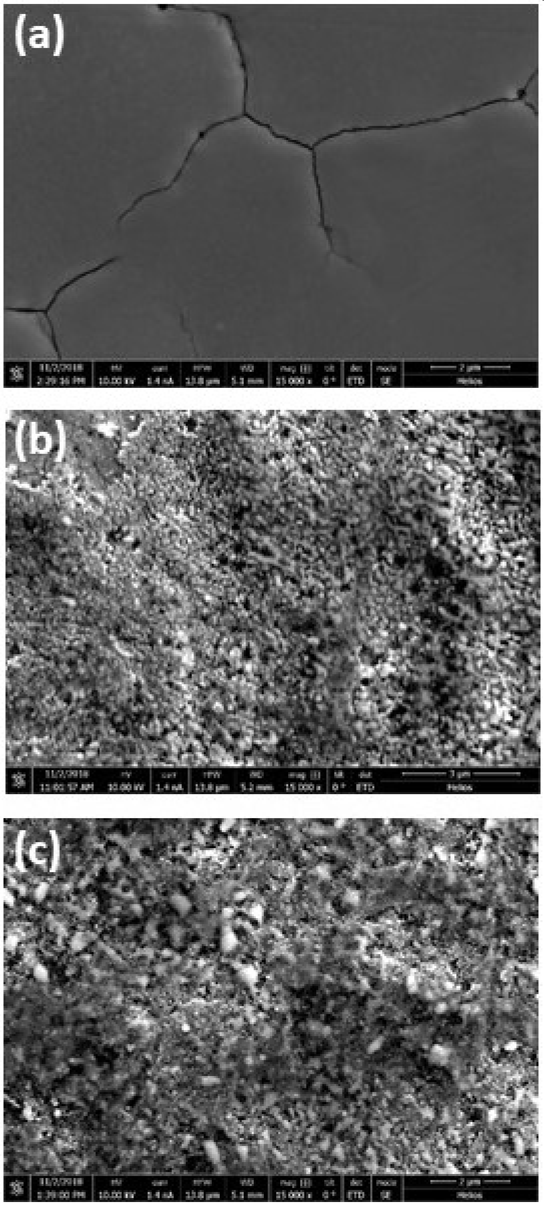

Fig. 9. Nd:YAG-shot steel irradiated with 310 shots per area at (a) 0.27 J/cm^2, (b) 1.15 J/cm^2, (c) 2.3 J/cm^2, all at 15,000× magnification.

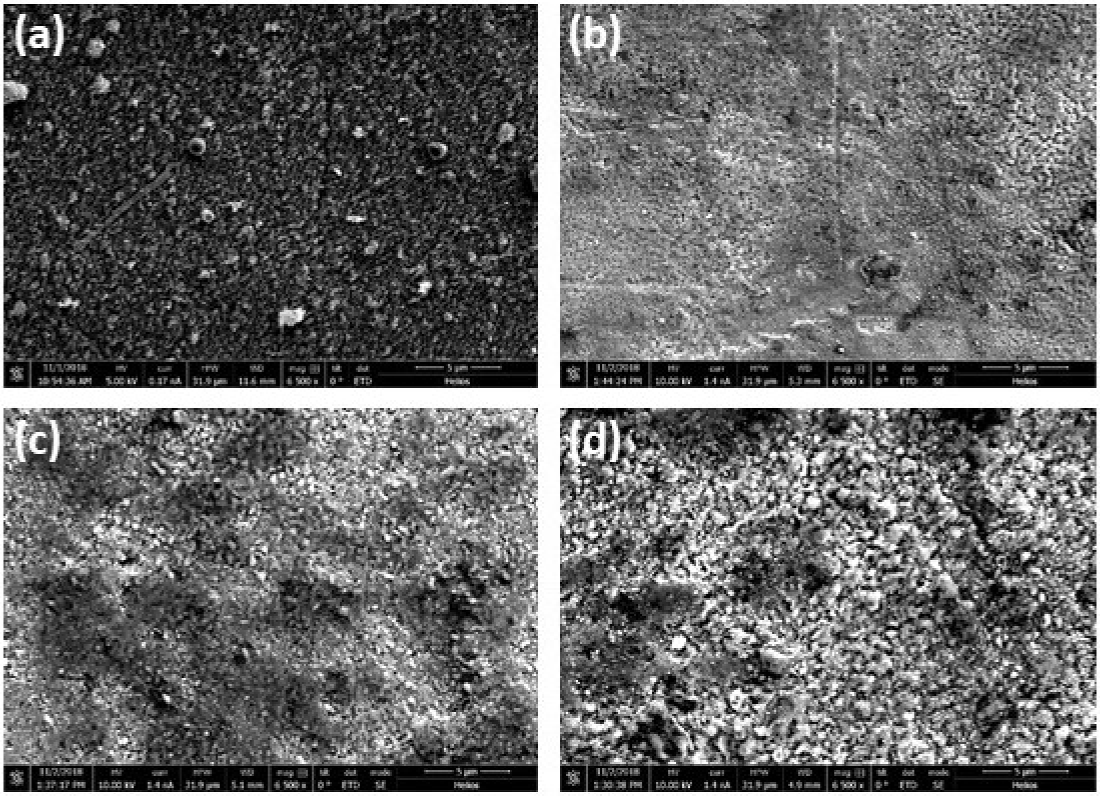

Fig. 10. Nd:YAG-shot steel irradiated at 2.3 J/cm^2 with (a) 80, (b) 120, (c) 310 and (d) 820 shots per area, all at 6500× magnification.

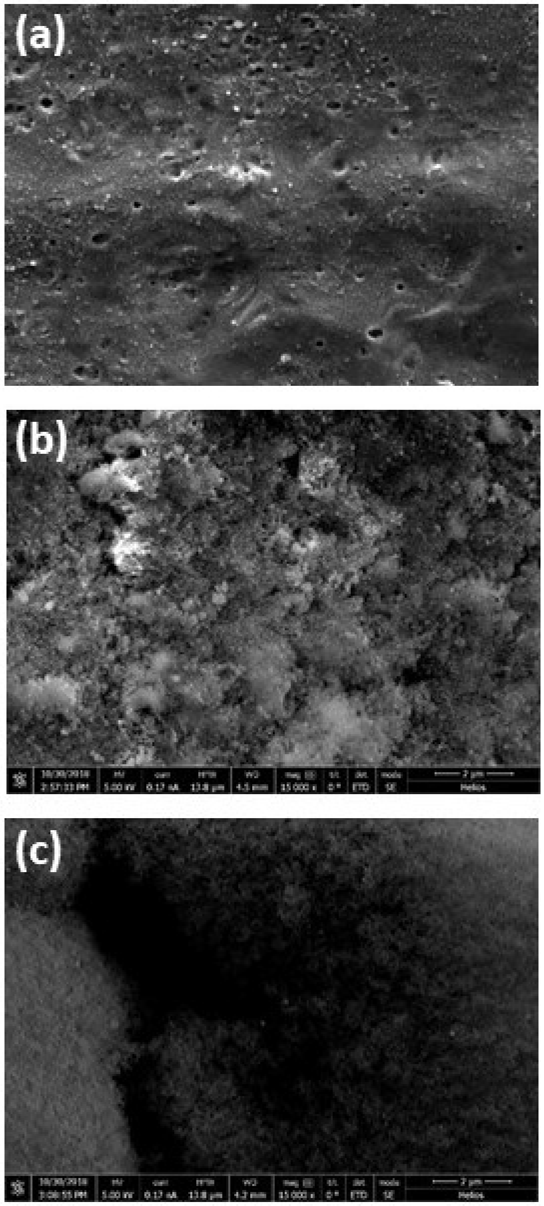

Fig. 11. Nd:YAG-shot Al irradiated with 310 shots per area at (a) 0.27 J/cm^2, (b) 1.15 J/cm^2, (c) 2.3 J/cm2, all at 6500× magnification.

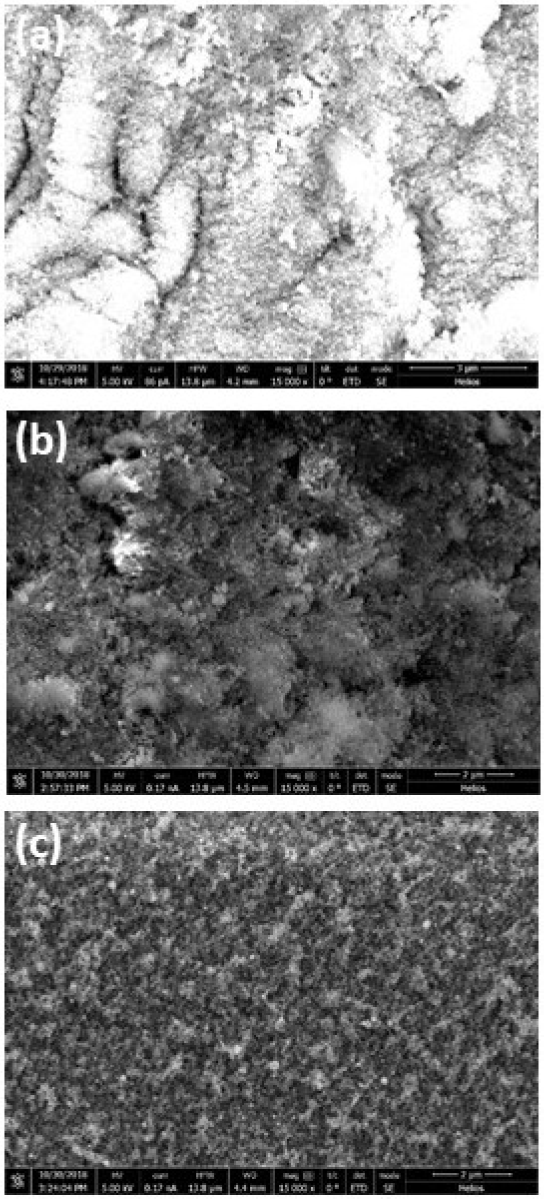

Fig. 12. Nd:YAG-shot Al irradiated at 1.15 J/cm^2, with (a) 120, (b) 310, and (c) 820 shots per area, all at 6500× magnification.

The range in the degree of overlap between shots is evident in Fig. 13, which shows Al irradiated with the KrF laser at three shot densities. All three show ridges that are parallel to the slow axis, but along the fast axis there is more topography at the lower shot density.

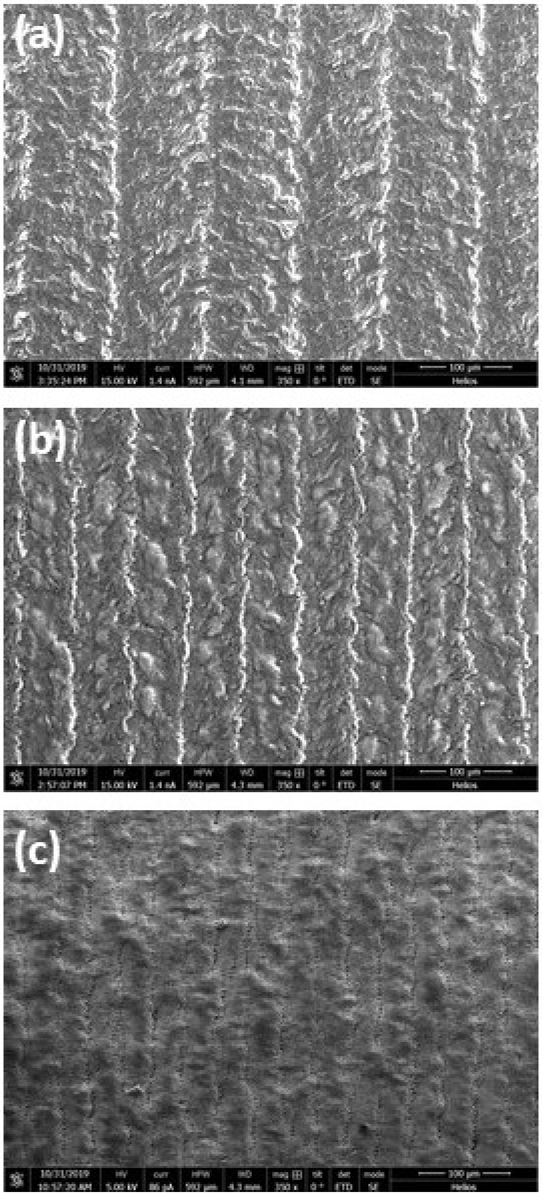

Fig. 13. Excimer-shot Al irradiated at 3.0 J/cm^2, with (a) 375, (b) 1000, and (c) 3000 shots per area, all at 350× magnification.

Discussion

The contact angle data show several noteworthy features, which the microscopy can help interpret.

First, the contact angles show considerable changes compared to the unirradiated material. The sample in the lower-left corner of each contour plot received the fewest shots per area and the lowest fluence, and shows the smallest topography change. These samples would be expected to show a contact angle closest to the unirradiated material, and with the exception of excimer-shot steel, which showed a contact angle of 95° compared to 79° for bare steel, this is observed. However, the contact angle deviates considerably from the unshot material as fluence, shot density, or both is increased. The fact that the lowest fluence and shot density yielded nearly no difference in contact angle suggests that the effect that dominates the contact angle behavior is a topographical effect rather than a chemical modification of the surface due to irradiation, or that if a chemical modification to the surface is important, it requires exceeding some threshold fluence to be achieved.

Second, the contact angle changes are non-monotonic in both laser fluence and shot density. For almost every fluence and shot density, following a line from low to high results in both increases and decreases in observed contact angle. Moreover, the observed contact angles are sometimes greater and sometimes less than the unirradiated material.

If we draw a horizontal line across the two panels of Fig. 1 at 1500 shots per area, and look at the topography as a function of fluence, the resulting comparisons are shown in Fig. 14 and Fig. 15, for steel and Al, respectively. Both show a progression from a relatively smooth surface, to a surface with some undulations decorated with small-scale roughness, and finally a surface with large-scale features, also decorated with small-scale roughness. The surface of the lowest fluence, despite having some small-scale features, is reasonably smooth and therefore gives a comparable contact angle to the unshot surface. At intermediate fluence, the surface exhibits the two different length scales of roughness characteristic of the lotus leaf effect, and thus the maximum contact angle occurs for this condition. Finally, at high fluence, the large-scale surface so dominates the topography that the hydrophobic effect of the small-scale features is overwhelmed, and thus the surface has become hydrophilic.

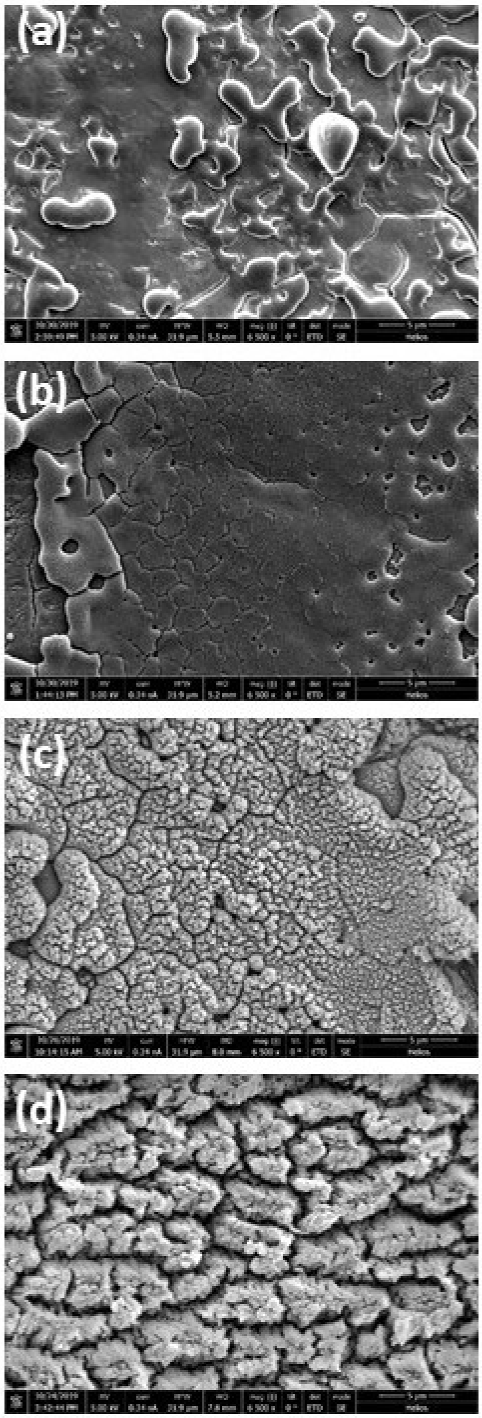

Fig. 14. Excimer-shot steel irradiated with 1500 shots per area at (a) 0.3 J/cm^2, (b) 1.0 J/cm^2, (c) 1.5 J/cm^2 and (d) 3.0 J/cm^2, all at 6500× magnification.

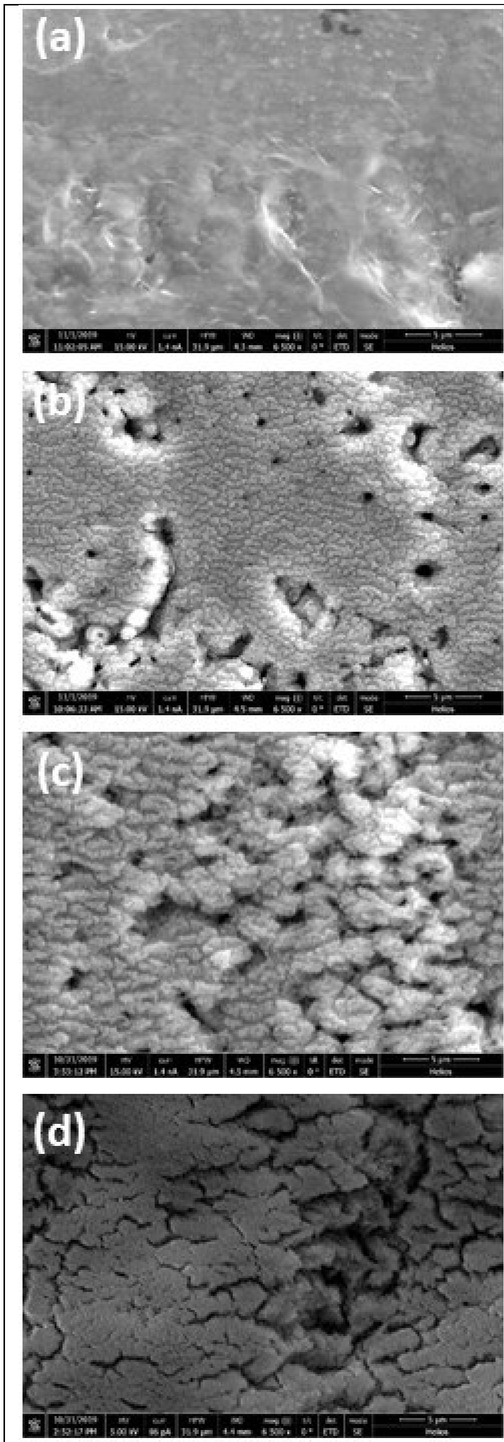

Fig. 15. Excimer-shot Al irradiated with 1500 shots per area at (a) 0.3 J/cm^2, (b) 1.0 J/cm^2, (c) 1.5 J/cm^2 and (d) 3.0 J/cm^2, all at 6500× magnification.

Relatedly, Fig. 16 shows four images, corresponding to the four circles shown in the inset. The 1.5 J/cm^2, 3000 shots per area sample and the 3 J/cm^2, 375 shots per area sample, have the highest contact angle, and these surfaces are the most similar, showing two length scales of surface roughness. The 1.5 J/cm^2, 375 shot per area sample also has a high contact angle, but appears to have only a single (small) length scale of surface feature. In contrast, the 3 J/cm^2, 3000 shot per area sample has a lower contact angle than unshot steel, and it has the largest length scale of roughness. This image corroborates the interpretation that surfaces with the right kind of surface topography become hydrophobic, while others become more hydrophilic, and that different laser conditions can induce similar surface conditions. Even though the top left and bottom right surface do not look *identical* – clearly these are different surfaces – they are sufficiently comparable with respect to having the needed two length-scales of roughness that they produce similar effects when subjected to wetting.

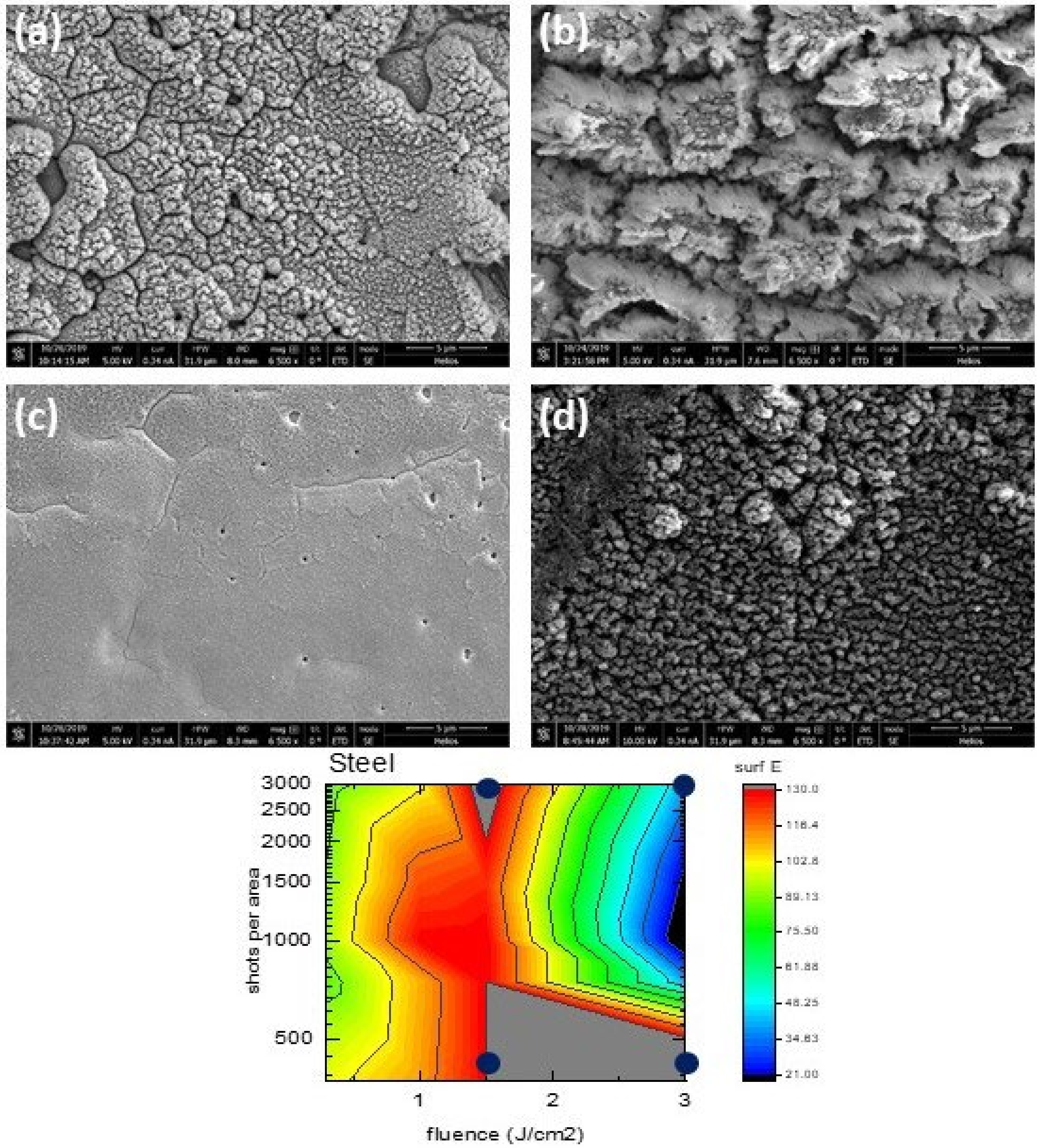

Fig. 16. (a)-(d) Excimer-shot steel, all at 6500× magnification. (a) 1.5 J/cm^2, 3000 shots per area; (b) 3.0 J/cm^2, 3000 shots per area; (c) 1.5 J/cm^2, 375 shots per area; (d) 3.0 J/cm^2, 375 shots per area. Lower panel: contour plot from Fig. 1; dots show the conditions corresponding to the images in (a)-(d).

Third, the surface is more hydrophobic when irradiated with 248 nm light than with 532 nm light. Fig. 17 provides some insight into this finding. The top row shows irradiated steel while the bottom row shows irradiated Al; the left shows irradiations at 532 nm and the right at 248 nm. The fluence and shot density are comparable. For both materials, the 532 nm samples are less hydrophobic than unshot material, whereas the 248 nm samples are more hydrophobic than unshot material. Comparing the left and right columns show that the topography is different for the different laser wavelengths.

Although the 532 nm samples show significant roughness, this is consistent with a single length scale of roughness, which appears to result in increased wettability. In contrast, the 248 nm samples are more consistent with two length scales, although the small-scale roughness of the steel sample is very fine.

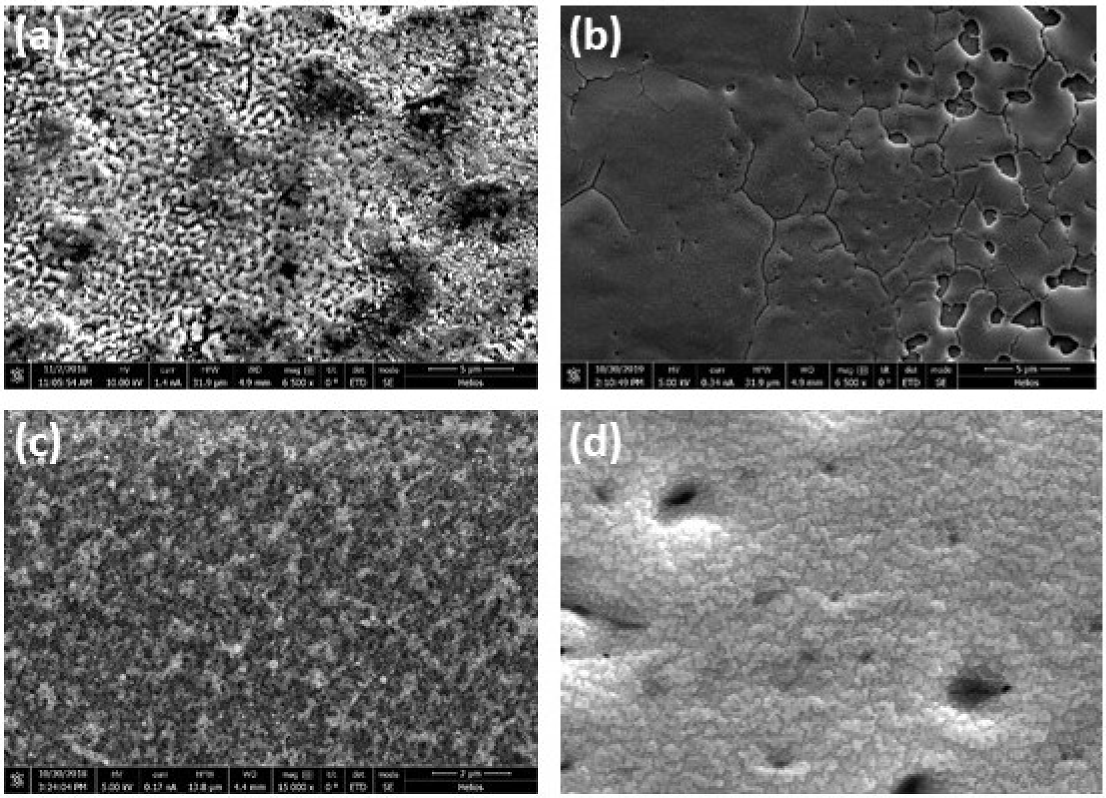

Fig. 17. (a) and (b) steel, (c) and (d) Al. Left side: Nd:YAG at 1.15 J/cm^2, 820 shots per area. Right side: Excimer at 1.0 J/cm^2, 750 shots per area. All at 6500× magnification.

An explanation for this discrepancy is not readily available. The skin depth of Al at 248 nm and 532 nm is 0.24 nm and 0.31 nm, respectively. These are so similar, and so short compared to the length scale of the roughness, that it is unlikely that differences in the absorption depth of the light can account for the topographical differences. Another possibility is that the slight pulse duration difference (15 ns for the 248 nm laser vs. 5 ns for the 532 nm laser) could lead to differences. The form this could take might be interaction of the laser beam with the ablation plasma, which is known to occur with ns lasers. This would be more pronounced in the longer 248 nm pulse. We observed that beam occlusion by the ablation plume significantly changed the surface morphology of polymer composite targets irradiated with a ms pulse laser [14]. In a different study, irradiation by a scanned ns laser of a metal target also showed differences as the scanning speed and pulse energy are varied. [15] In that case, the laser pulse rate was 200 kHz compared to 10 Hz in the experiments reported here, and so in the Ref. [15] experiments, the plume was still present before the arrival of the next pulse.

The best way to investigate whether the pulse duration contributes significantly would be to use one of the other harmonics of the Nd:YAG laser, such as 355 nm or 266 nm. If the resulting surface morphology looked more comparable to the 532 nm-irradiated surface, this would strongly indicate that pulse duration, and not wavelength, dominated the surface topography effect.

Ref. [15] also notes how the degree of overlap influences the topography of the irradiated area. When there is sufficient overlap between subsequent shots, ablation becomes effectively continuous with a 200 kHz laser. But even with a low-pulse rate laser, the difference between spots that almost entirely overlap and those that only partially overlap can be considerable. In the former case, the centers of the ablation craters are nearly concentric, whereas in the latter case, the center of the ablation craters are far apart, leading to the formation of a ridge between the two adjacent craters.

This phenomenology can be observed in Fig. 13, a high fluence series in which the shot density is varied. At the lowest shot density (375 shots per area), the ridges perpendicular to the slow axis are defined but the curvature of individual spots along the fast axis are also evident. These are less pronounced at intermediate shot density (1000 shots per area) and washed out entirely at high shot density (3000 shots per area). However, the absolute fluence also plays a role in setting the crater depth, as the comparison in Fig. 18 makes clear. The sample in the upper panel was irradiated at a lower fluence, and shows fine-scale particles but no large surface undulations, whereas the sample in the lower panel was irradiated at high fluence and shows larger undulations and larger-scale particles decorating those undulations, and correspondingly, the higher fluence sample shows enhanced hydrophobicity whereas the lower fluence sample’s hydrophobicity is comparable to the baseline.

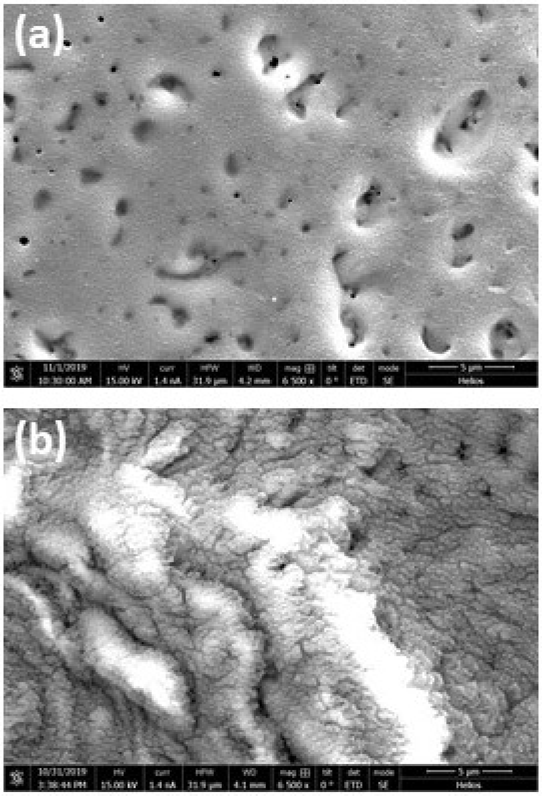

Fig. 18. Excimer-shot Al irradiated with 375 shots per area at (a) 1.0 J/cm^2 and (b) 3.0 J/cm^2, all at 6500× magnification.

Conclusion

Aluminum and steel test panels were irradiated with nanosecond pulsed lasers at 248 nm and 532 nm at varying shot densities. The surface topography was measured with electron microscopy, and showed combinations of long length scale undulations and ridges and small length scale particles, with the relative amount of each type of feature depending on the laser conditions. Measurements of the contact angle of water showed that some surfaces become more hydrophobic after irradiation and some became less. There is agreement between the microscopy and surface topography in that surfaces that showed two length scales of roughness were more likely to exhibit enhanced hydrophobicity than those that exhibited only one length scale, consistent with the familiar Lotus leaf effect.

Future work could seek to apply coatings to these surfaces, to ascertain whether the surfaces improve or hinder the coating's ability to bond well to the surface.

References

[1] Aircraft maintenance technician's manual, Publication FAA-8083, Federal Aviation Administration.

[2] J.A. Callow and M.E. Callow, "Trends in the development of environmentally friendly fouling-resistant marine coatings", *Nature Communications* **2**, 244 (2011).

[3] D.E. Barlow *et al.*, "Characterization of the adhesive plaque of the barnacle *Balanus Amphitrite*: amyloid-like nanofibrils are a major component," *Langmuir* **26**, 6549 (2010).

[4] G.H. Dickinson *et al.*, "Barnacle cement: a polymerization model based on evolutionary concepts", *J. Experimental Biology* **212**, 3499 (2009).

[5] G.D. Bixler, "Bioinspired surface for low-draw self-cleaning and antifouling: shark skin, butterfly and rice leaf effects", *Ph.D. thesis*, The Ohio State University (2013).

[6] Crouch *et al*, "Comparison of structure and properties of femtosecond and nanosecond structured silicon", *Appl. Phys. Lett.* **84** 1850 (2004).

[7] Etsion, "State of the art in laser surface texturing", *J. Tribology* **127** 248 (2005).

[8] Wong and Liang, "Effect of laser melting treatment of the structure and corrosion behavior of Al and Al-Si alloys", *J. Mat. Proc. Tech.* **63** 930 (1997).

[9] Yue *et al.*, "Excimer laser surface treatment of aluminum alloy AA7075 to improve corrosion resistance", *Surf. Coat. Tech.* **179** 158 (2004).

[10] Peyre *et al.*, "Surface modifications induced in 316L steel by laser peening and shot-peening; influence on pitting corrosion resistance", *Mat. Sci. Eng.* **A280** 294 (2000)

[11] Watkins *et al*., "Microstructure and corrosion properties of laser surface processed aluminum alloys, a review", *Mat. Sci. Eng.* **A231** 55 (1997)

[12] Tang *et al*., "Laser ablation of metal substrates for super-hydrophobic effect", *J. Laser Micro/Nanoeng.* **6** 6 (2011).

[13] Thieme *et al*., "Generation of ultrahydrophobic properties of aluminum – a first step to self-cleaning transparently coated metal surfaces", *Adv. Eng. Mat.* **3** 691 (2001).

[14] S.F. Bartolucci *et al.*, "Infrared laser ablation of polymeric nanocomposites: a study of surface structure and plume formation", *J. Appl. Phys.* **120**, 225103 (2016).

[15] J. Yuan *et al.*, "Experimental study on the laser-matter-plume interaction and its effects on laser ablation during nanosecond scanning ablation process", *Opt. Expr.* **27**, 23204 (2019).